NASA TN D-1936

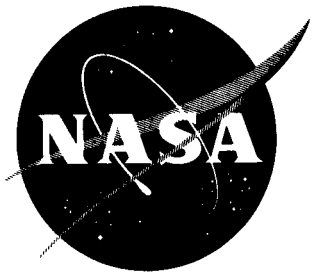

TECHNICAL NOTE

D-1936

TRAILBLAZER I REENTRY-BODY WIND-TUNNEL TESTS AT A MACH NUMBER OF 6.7 WITH THEORETICAL AERODYNAMICS AND A LIMITED DYNAMIC ANALYSIS

By Herbert R. Schippell

Langley Research Center
Langley Station, Hampton, Va.

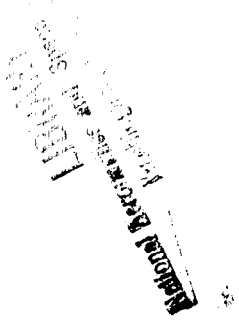

NATIONAL AERONAUTICS AND SPACE ADMINISTRATION

WASHINGTON July 1963

NATIONAL AERONAUTICS AND SPACE ADMINISTRATION

TECHNICAL NOTE D-1936

TRAILBLAZER I REENTRY-BODY WIND-TUNNEL TESTS AT A MACH NUMBER OF 6.7 WITH THEORETICAL AERODYNAMICS AND A LIMITED DYNAMIC ANALYSIS

By Herbert R. Schippell

SUMMARY

The aerodynamic forces and moments of scale models of a Trailblazer I reentry configuration were experimentally determined in the Langley 11-inch hypersonic wind tunnel at a Mach number of 6.7 in air. The reentry configuration is basically a 5-inch-diameter sphere with an aft-mounted short cylindrical appendage of less diameter than the sphere.

The data obtained from the tests compare favorably with predictions made by a modified Newtonian theory, and the tests show that the configuration is statically unstable up to an angle of attack of about 30° and becomes statically stable near an angle of attack of 90°. A limited theoretical analysis of the reentry body motions using the measured data shows that the aerodynamic moments interact with the body gyroscopic moments and result in maximum angles of attack at maximum dynamic pressures.

INTRODUCTION

The need for basic knowledge relative to high-speed objects reentering the earth's atmosphere has stimulated many theoretical and experimental programs. One phase of study selected was to determine the radar cross section and radiation properties of the ionized trail during an actual atmospheric reentry when the weight and geometry of the reentry body is known.

Trailblazer I, an inexpensive six-stage rocket vehicle, was designed with this aim in mind. The vehicle delivers a reentry body downward into the earth's atmosphere at a speed near a Mach number of 20 and allows the reentry event to be observed by various radar and optical instruments and the unaided eye. The Trailblazer I trajectory is unusual in that the reentry rocket stages are fired downward on a near vertical trajectory from high altitude. The trajectory is accomplished by assembling the six rocket stages with the last three pointed backward, in a retro attitude, toward the first three stages. These last three stages are contained in a spin-stabilized velocity package and are rocketed out

the open base of the package near an altitude of 10^6 feet. The final stage utilizes a specially designed 5-inch-diameter spherical rocket motor to achieve the needed high velocity increment. The experimental reentry body is the empty spherical rocket motor with a torus telemeter encircling the exhaust nozzle.

The initial conditions of motion assumed for the spinning reentry body are an angle of attack of 14° and a superimposed fluctuation of 7°. These initial motion conditions are estimated from a consideration of the trajectory scheme and the six stages of rocket thrust misalinement, unbalance, and tip-off. During the atmospheric portion of the reentry body's flight, the aerodynamic and gyroscopic moments are in opposition and the net result determines the body motions. It is believed that body motion and angle of attack have an appreciable effect on the observed reentry phenomena and, since the reentry configuration was estimated to be aerodynamically unstable, it was considered necessary to determine its aerodynamic characteristics.

The purpose of this paper is to present the results of wind-tunnel force tests conducted in the Langley 11-inch hypersonic tunnel with two scale models of the Trailblazer I reentry body. Also, the pertinent modified Newtonian theory and results of a limited analytical study of the dynamical reentry motions are included. Tests were conducted at a Mach number of 6.7 in air for Reynolds numbers between approximately 0.1×10^6 and 0.5×10^6 based on maximum body diameter, and the angle-of-attack range was varied between -2° and 116°.

SYMBOLS

The moment center was located 0.8D behind the nose and corresponds to the empty center-of-gravity location of the prototype as noted in figure 1(a). The coefficients are based on the maximum body diameter and cross section and referenced to the empty center of gravity.

C_A axial-force coefficient, $\frac{\text{Axial force}}{qS}$

C_m pitching-moment coefficient, $\frac{\text{Pitching moment}}{qSD}$

C_{m_α} pitching-moment-curve slope

C_N normal-force coefficient, $\frac{\text{Normal force}}{qS}$

C_{N_α} normal-force-curve slope

$C_{p,max}$ maximum pressure coefficient

D maximum body diameter

h	altitude, ft
M	Mach number
p_t	total tunnel pressure, lb/sq ft
q	dynamic pressure, lb/sq ft
R	Reynolds number, based on body maximum diameter
S	maximum cross-sectional area of body
T_t	total tunnel temperature, $^{\circ}R$
V	velocity, ft/sec
x	distance along X-axis from center of gravity (unless otherwise noted), ft
X	axis coincidental with model center line
Z_e	radius of earth extended
α	angle of attack, deg
β	angle of sideslip, deg
γ	flight-path angle (measured from vertical), deg
η	total yaw angle, $\sqrt{\alpha^2 + \beta^2}$, deg

Subscripts:

max	maximum
min	minimum

APPARATUS AND TESTS

Tunnel

The tests were made in the Langley 11-inch hypersonic tunnel. This tunnel utilizes fixed-geometry interchangeable nozzles to facilitate testing at different Mach numbers. The details of the air nozzle that was used here are reported in reference 1 and a general description of the remainder of the tunnel is contained in reference 2.

Model

The Trailblazer I reentry body is a 5.05-inch-diameter spherical rocket motor with a torus telemeter contained in an aft-mounted short circular cylinder

surrounding the motor nozzle. The geometry of the prototype and the wind-tunnel models is shown in the sketch of figure 1. The two wind-tunnel models are designated models 1 and 2 and photographs of these are given as figure 1(b). The models were made as large as possible to use as much of the working range of the wind-tunnel balance as possible and be consistent with tunnel-starting requirements. Model 2 was made slightly smaller than model 1 to prevent tunnel blockage when starts were made at $\alpha = 90^{\circ}$. The sting mounting hole of model 2 was perpendicular to its longitudinal center line and passed through the empty center-of-gravity location.

Tests

The tunnel test conditions for the different models are as follows:

Test	Model	p_t	T_t	M	R	Range of α
1	1	1.058×10^4	1,130	6.6	0.18×10^6	-2° to 59°
2	1	2.530	1,080	6.7	.45	-2° to 59°
3	2	1.058	1,055	6.7	.15	60° to 114°
4	2	1.481	1,010	6.7	.19	60° to 114°

The test-section Mach number varies slightly with tunnel stagnation pressure because of changes in boundary-layer thickness. Mach number was recorded at every data point and the average for each test is shown in the table. This average Mach number has an accuracy of ± 0.04 and this range of accuracy includes all the data points measured. Reynolds number is obtained by computing the equilibrium expansion of air from the pressure and temperature conditions shown.

Precision of Data

The force measurements were made with two different six-component strain-gage balances, only three components of which were needed during each test. These gages were constructed to provide an accuracy of 1/2 percent at full load. For angles of attack of 28° and less, model 1 was tested on a balance that has a load capability of 15 pounds axial force, 10 pounds normal force, and 15 inch-pounds pitching moment. For angles of attack of 30° and above, all tests were conducted on a balance that had load capabilities of 10 pounds axial force, 16 pounds normal force, and 16 inch-pounds pitching moment. The repeatability of the data is indicated by the scatter of the measured points. The angle of attack was measured optically by a prismatic mirror on the model. One additional source of error results from base pressure. Base-pressure measurements were made at three different points across the base of model 1 for angles of attack from -2° to 59° and these measurements varied from free-stream pressure to about 1/2 free-stream pressure; hence, no base-pressure corrections were applied.

DISCUSSION OF RESULTS

A supporting theoretical analysis of the Trailblazer I aerodynamic characteristics was considered to be of interest. A Newtonian type of analysis was chosen with a similar body shape. The geometry of the Newtonian body used can be seen in figure 2. The Newtonian body is composed of a hemisphere-cylinder forebody and a cone-frustum—cylinder afterbody. The cone frustum, or forward part of the afterbody, is the principal geometric difference between the assumed Newtonian body and the full-scale reentry body. The small portion protruding from the base is entirely omitted on the Newtonian body and the base is assumed to be a flat circular disk. The Newtonian solution for a hemispherical nose shape is found in reference 3 and that for the backward-facing cone frustum is solved as part of a different configuration in reference 4. All Newtonian approximations are modified for Mach number after the manner suggested in reference 3; this modification amounts to using the pressure coefficient behind a normal shock instead of the Newtonian value of $C_{p,max} = 2$. The results of the modified Newtonian computations are compared with the measured wind-tunnel data in the appropriate figures.

Duplication of Prototype Mach Number and Reynolds Number

It is not possible to obtain wind-tunnel data for the entire range of reentry Mach number and Reynolds number encountered with the Trailblazer I reentry body. These data are for a single Mach number with some variation in Reynolds number. Figure 3 shows the variation of Reynolds number with Mach number for the theoretical trajectory of the Trailblazer I reentry body with relation to the tunnel test data. The test Reynolds numbers bracket those of the prototype flight conditions.

Aerodynamic Coefficients

Normal force.- The variation of normal-force coefficient with angle of attack is shown in figure 4. The test data show a slight mismatch at an angle of attack near 60° and this mismatch corresponds to the angle of attack at which model 2 was substituted for model 1. The exact explanation for this disagreement is not known but base-pressure effects and interference of the sting with the pressure distribution of model 2 could possibly be a cause. The agreement throughout the entire angle-of-attack range of the experimental and theoretical data is good.

Axial force.- The variation of axial-force coefficient for all data is shown in figure 5. Although the test data are slightly below the theoretical data at an angle of attack near 0°, the agreement generally is very good.

Pitching moment.- The pitching moment of the Trailblazer I model was difficult to measure accurately, because of the small forces on this component of the balance. The scatter of the data presented in figure 6 indicates its repeatability. The test data show the model to be statically unstable below an angle of attack of 30° and to exhibit a trend toward stability at the higher angles of attack. Theory predicts the trend of experiment from $\alpha = 0^\circ$ to near $\alpha = 55^\circ$. For angles above $\alpha = 55^\circ$, the theory diverges from the experimental data in that

the theory predicts stability up to about $\alpha = 105^{\circ}$ and experiment shows neutral stability up to an angle of attack of about 85°. It was not possible to determine just what part of the disagreement is caused by measuring accuracy and what part is caused by the inability of the theory to predict the proper aerodynamic coefficients. The static stability parameter, C_m plotted against C_N, is shown in figure 7(a). Figure 7(b) is a plot of the center-of-pressure location in body diameters from the nose as a function of the angle of attack. This figure shows no appreciable Reynolds number effects over the range tested. Near $\alpha = 0^{\circ}$ the center-of-pressure location was obtained by use of the slopes C_{N_α} and C_{m_α}. Figure 7(b) also shows graphically the small static margin in the α range where stability does exist.

Flow-Field Characteristics

Figure 8 is a sketch of the various elements of the flow field that were observed in schlieren photographs at $\alpha = 0^{\circ}$ and illustrates the position of the base-pressure tubes. The flow-field elements are named by using the nomenclature of reference 5. The sketch shows the approximate location of the pressure tubes near the base of model 1 and the open end of the base-pressure tubes was approximately 0.025 inch from the base and did not touch the model throughout the test. The wake is drawn to originate at the forebody-afterbody juncture as indicated in the schlieren photographs in figure 9. The shock standoff distance at $\alpha = 0^{\circ}$ is measured to be 0.07D. The sketch has been included because resolution of the various flow-field elements is lost from the schlieren photographs of figure 9 during reproduction.

Figure 9 is compiled of various schlieren photographs that were taken during the test and illustrates the shock-wave shape for increments of about 10° in angle of attack. A definition of the shock shape that accompanies a reentry is necessary before a thermodynamic understanding of the flow field that surrounds the body can be gained. One way to obtain these data is to measure the shock standoff distance and shape from a schlieren photograph of known test conditions.

Dynamic Analysis

A better understanding of the reentry body's motions is needed in order to evaluate the experimental data obtained in free flight. Before the actual reentry body's motion is discussed, it is felt necessary to call attention to the unusual initial orientation of the reentry body in space. The reentry body is placed in this position in space and given its velocity by the unique rocketry system of the Trailblazer I vehicle. An unusual trajectory results from assembling this six-stage rocket with the last three stages pointed backward in a retro attitude and is shown in figure 10. The flow field that surrounds the reentry body also varies in a complex manner. Some understanding of the variation of this flow field with motions of the reentry body during all phases of reentry is also desirable.

In general, the descent motion of the reentry body may have another motion superimposed on it. This superimposed motion may be a random tumble, a periodic oscillation, or a spin with some kind of precession. The Trailblazer I reentry body is spin-stabilized to within certain limits. The vehicle was designed and is believed to place the reentry body into motion oriented as is shown in figure 11. This figure shows that the vehicle center line is oriented to one side of the total velocity vector and illustrates the total yaw angles that were chosen as initial machine conditions near an altitude of 3×10^6 feet during reentry. The precession cone in the figure is described by the motion of the reentry-body center line as the body spins about its longitudinal axis at 39 cycles per second and precesses about the cone center line with no nutation.

In order to understand these combined reentry motions, a six-degree-of-freedom motion analysis was performed with an IBM computer. The equations and computer program details are described in reference 6. The aerodynamic data that were obtained in these tests and put into the computer are shown in figure 12. The additional mass characteristics and initial conditions that were used are given in the appendix.

The computer results of interest are shown in figure 13 as plots of total yaw angle and dynamic pressure against altitude. Briefly, the force system involved is composed of the body gyroscopic moments and aerodynamic moments. In effect, the analysis shows the manner in which the total yaw angle is changed by the interaction of the gyroscopic and aerodynamic moments during descent through the atmosphere. The total yaw angle increases very rapidly as dynamic pressure increases and in the example reaches a maximum value of 49° at a maximum dynamic pressure of 16.9 pounds per square foot at an altitude of approximately 115,000 feet. At lower altitudes the dynamic pressure decreases which in turn permits the gyroscopic moments to decrease the total yaw angle.

CONCLUSIONS

An analysis of the experimental data obtained at $M = 6.7$ in air from tests in the Langley 11-inch wind tunnel on scale models of the Trailblazer I reentry configuration lead to the following conclusions:

1. As was anticipated, the test data show that the reentry body is statically unstable up to an angle of attack of about 30° and then show a trend toward stability at higher angles.

2. A modified Newtonian theory adequately predicts the measured axial- and normal-force coefficients. The pitching-moment trend is predictable by the theory at angles of attack between 0° and 55° but the test data differ from the theory at higher angles.

3. A limited analysis of the reentry body motions shows that the total yaw angle reaches a maximum of less than 50° at the altitude corresponding to maximum dynamic pressure.

Langley Research Center,
National Aeronautics and Space Administration,
Langley Station, Hampton, Va., May 3, 1963.

APPENDIX

COMPUTER INFORMATION

The computer program that was used has provisions for a description of an atmosphere and aerodynamic dampening. No aerodynamic dampening was considered and a standard 1959 ARDC atmosphere was used. All quantities of computer input not listed below or previously stated in the text were chosen to be zero.

Center-of-gravity location, body diameters aft of nose	0.80
Weight, lb	1.79
Roll inertia, slug-ft^2	0.00111
Pitch, yaw inertia, slug-ft^2	0.00250
Gravity, ft/sec^2	31.869
Reference area, sq ft	0.1363542
Reference length, ft	0.41667
Longitudinal velocity component, ft/sec	20,184.75
Velocity component in yaw plane, ft/sec	0
Velocity component in pitch plane, ft/sec	2,473.691
Horizontal range, ft	-497,000
Altitude, ft	-300,000
Flight-path angle, radians	-1.276
Roll rate, radians/sec	245.0
Yawing velocity, radians/sec	-13.7696

REFERENCES

1. Bertram, Mitchel H.: Exploratory Investigation of Boundary-Layer Transition on a Hollow Cylinder at a Mach Number of 6.9. NACA Rep. 1313, 1957. (Supersedes NACA TN 3546.)

2. McLellan, Charles H., Williams, Thomas W., and Beckwith, Ivan E.: Investigation of the Flow Through a Single-Stage Two-Dimensional Nozzle in the Langley 11-Inch Hypersonic Tunnel. NACA TN 2223, 1950.

3. Wells, William R., and Armstrong, William O.: Tables of Aerodynamic Coefficients Obtained From Developed Newtonian Expressions for Complete and Partial Conic and Spheric Bodies at Combined Angles of Attack and Sideslip With Some Comparisons With Hypersonic Experimental Data. NASA TR R-127, 1962.

4. Dickey, Robert R.: Forces and Moments on Sphere-Cone Bodies in Newtonian Flow. NASA TN D-1203, 1961.

5. Love, Eugene S.: Base Pressure at Supersonic Speeds on Two-Dimensional Airfoils and on Bodies of Revolution With and Without Fins Having Turbulent Boundary Layers. NACA TN 3819, 1957. (Supersedes NACA RM L53C02.)

6. James, Robert L., Jr. (With appendix B by Norman L. Crabill): A Three-Dimensional Trajectory Simulation Using Six Degrees of Freedom With Arbitrary Wind. NASA TN D-641, 1961.

Table of dimensions

	a	b	c	d	e	f	g	h	i
Prototype	2.525	1.514	7.573	4.848	0.195	0.825	2.220	3.950	4.100
Model 1	1.500	0.896	4.496	2.875	0.116	0.490	1.319	2.346	2.430
Model 2	1.125	0.674	3.359	2.160	0.087	0.333	0.989	1.760	1.827

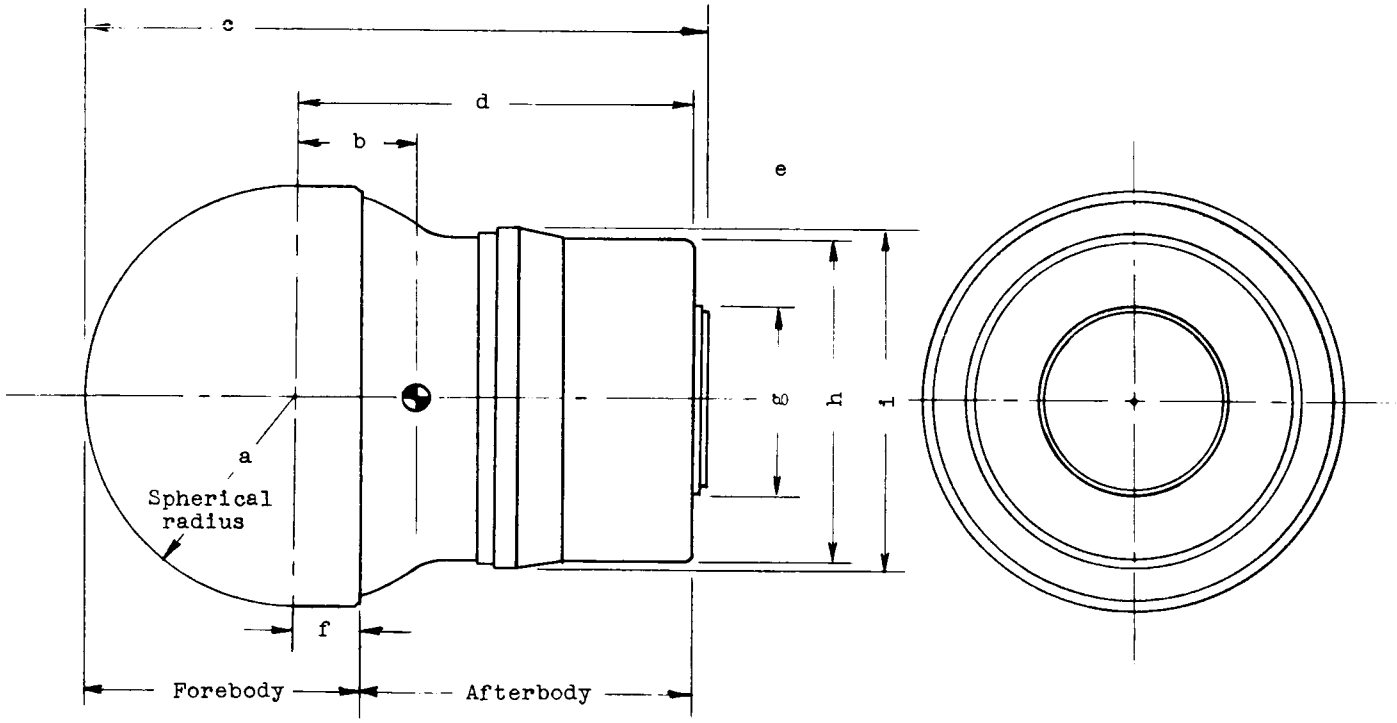

(a) Sketch illustrating principal dimensions and location of full-scale empty center of gravity.

Figure 1.- Reentry body models. All dimensions are in inches.

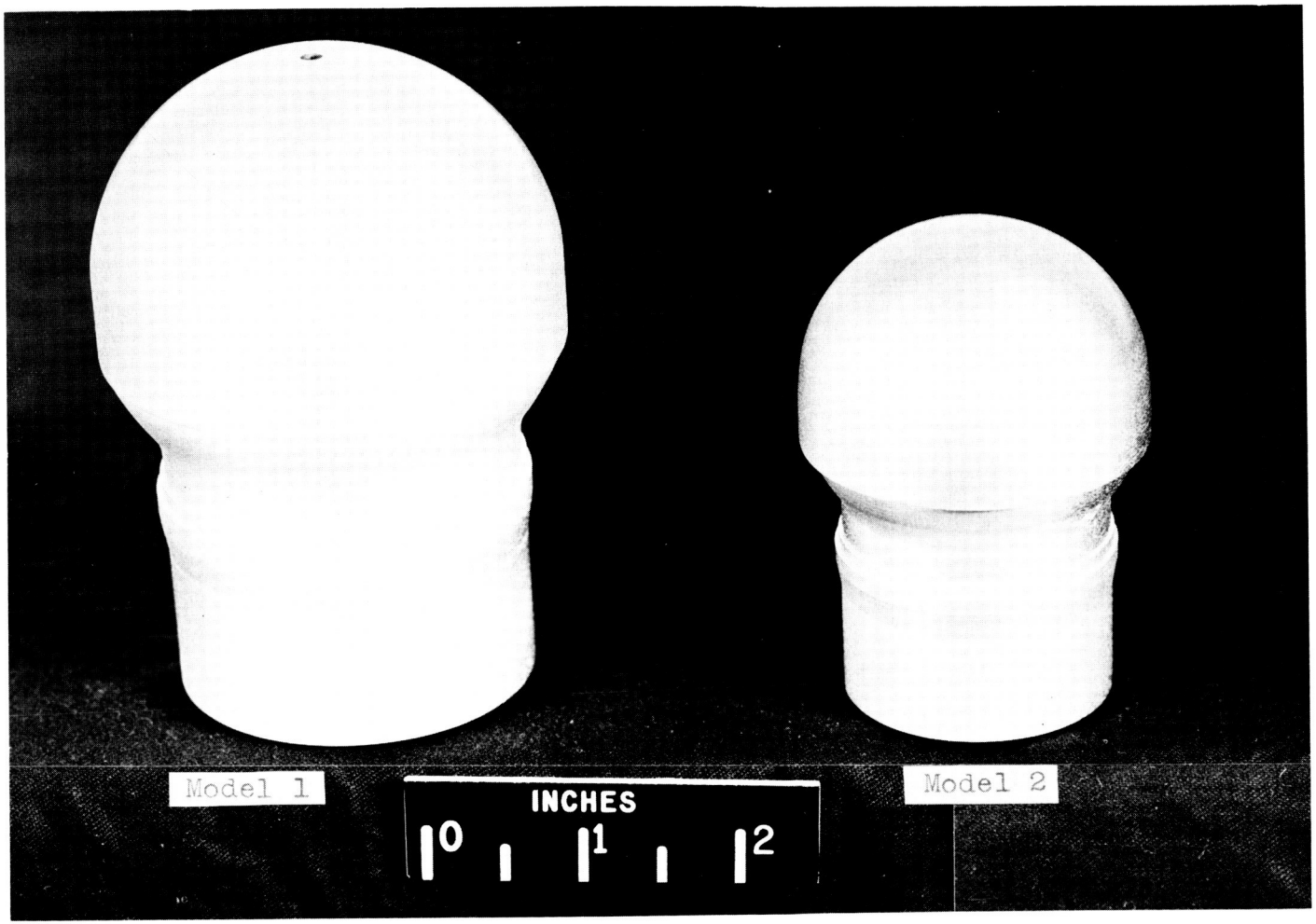

(b) Photograph of the two models. L-63-3114

Figure 1.- Concluded.

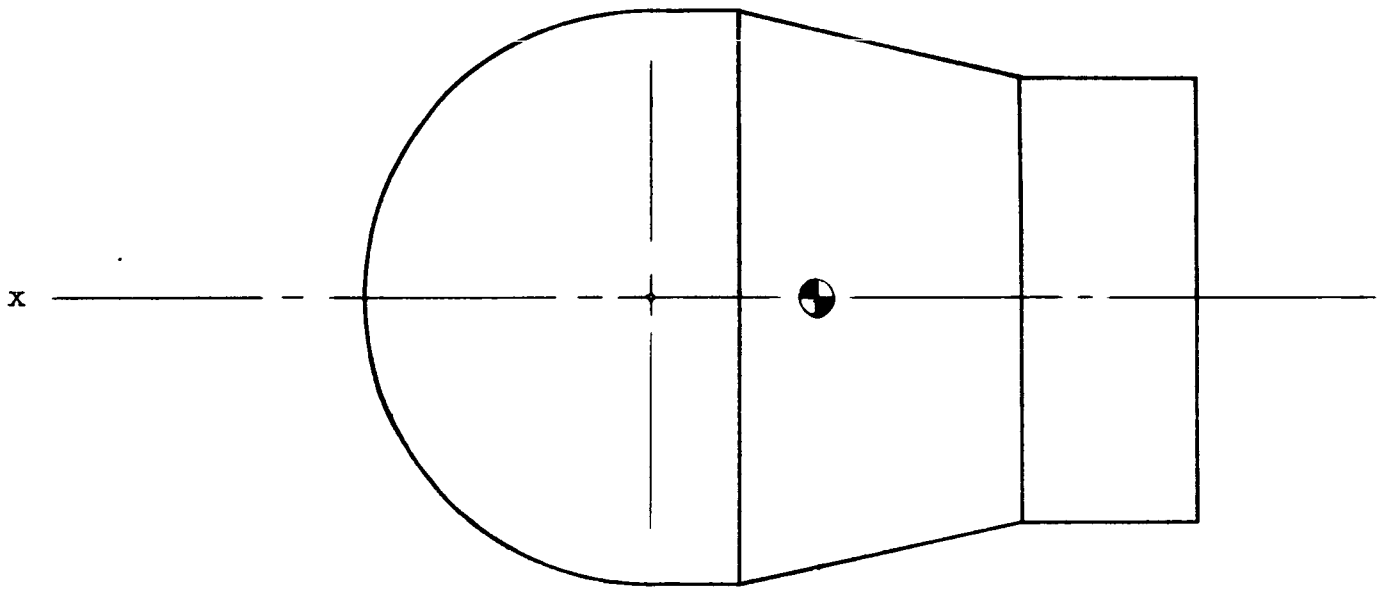

Figure 2.- The body shape assumed for the Newtonian analysis with the body-axis system shown.

Symbol	Test medium	Model
———	Theoretical trajectory	Prototype
○	Langley 11 inch tunnel, Air	Model - 1
□	Langley 11 inch tunnel, Air	Model - 2

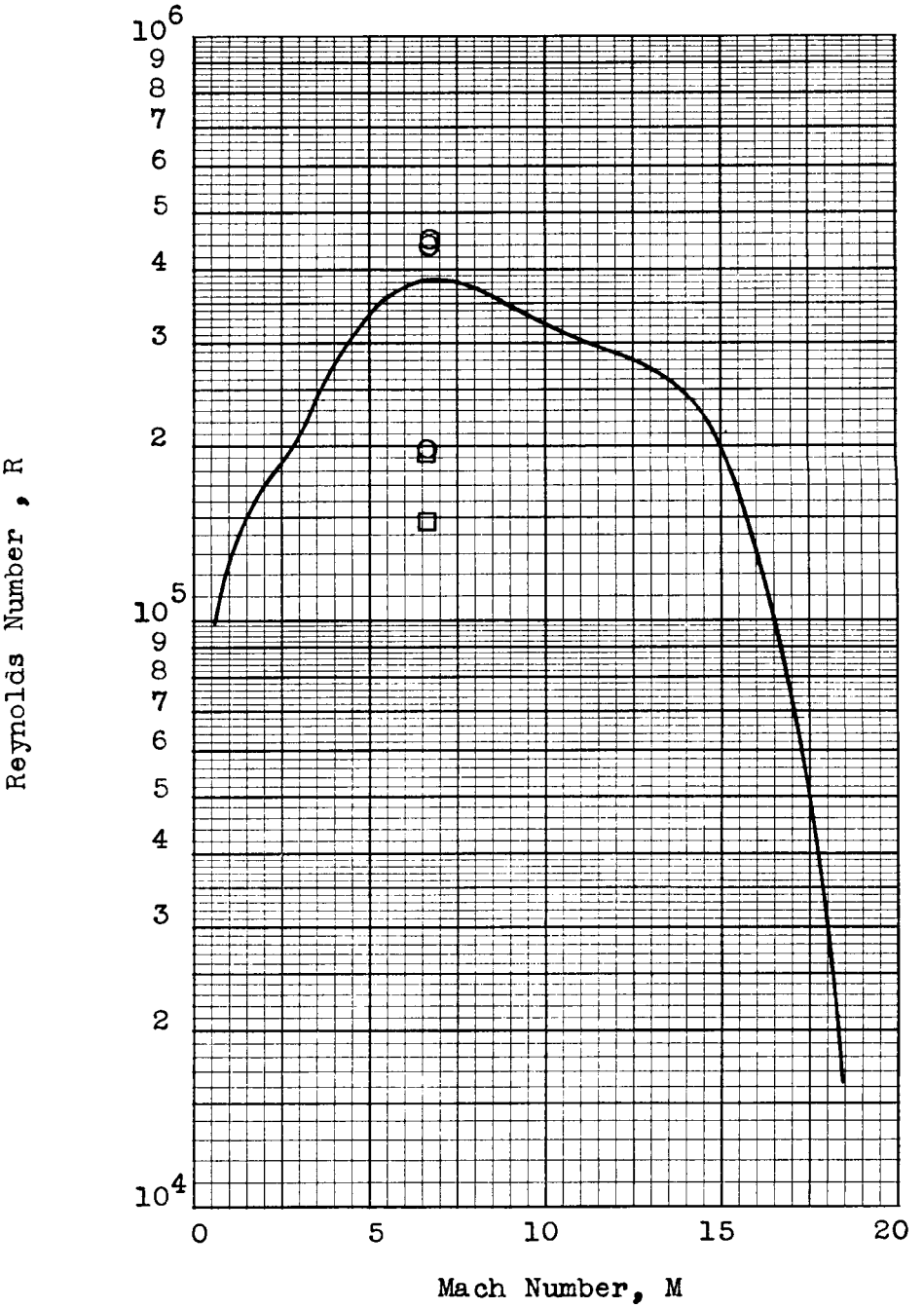

Figure 3.- Variation of Reynolds number with Mach number for a typical theoretical Trailblazer I reentry body trajectory with the tunnel test points indicated.

		M	R
Model 1,	○	6.6	0.18×10^6
	□	6.7	0.45×10^6
Model 2,	⌂	6.7	0.15×10^6
	△	6.7	0.19×10^6
Theory	-------	7.0	Modified Newtonian

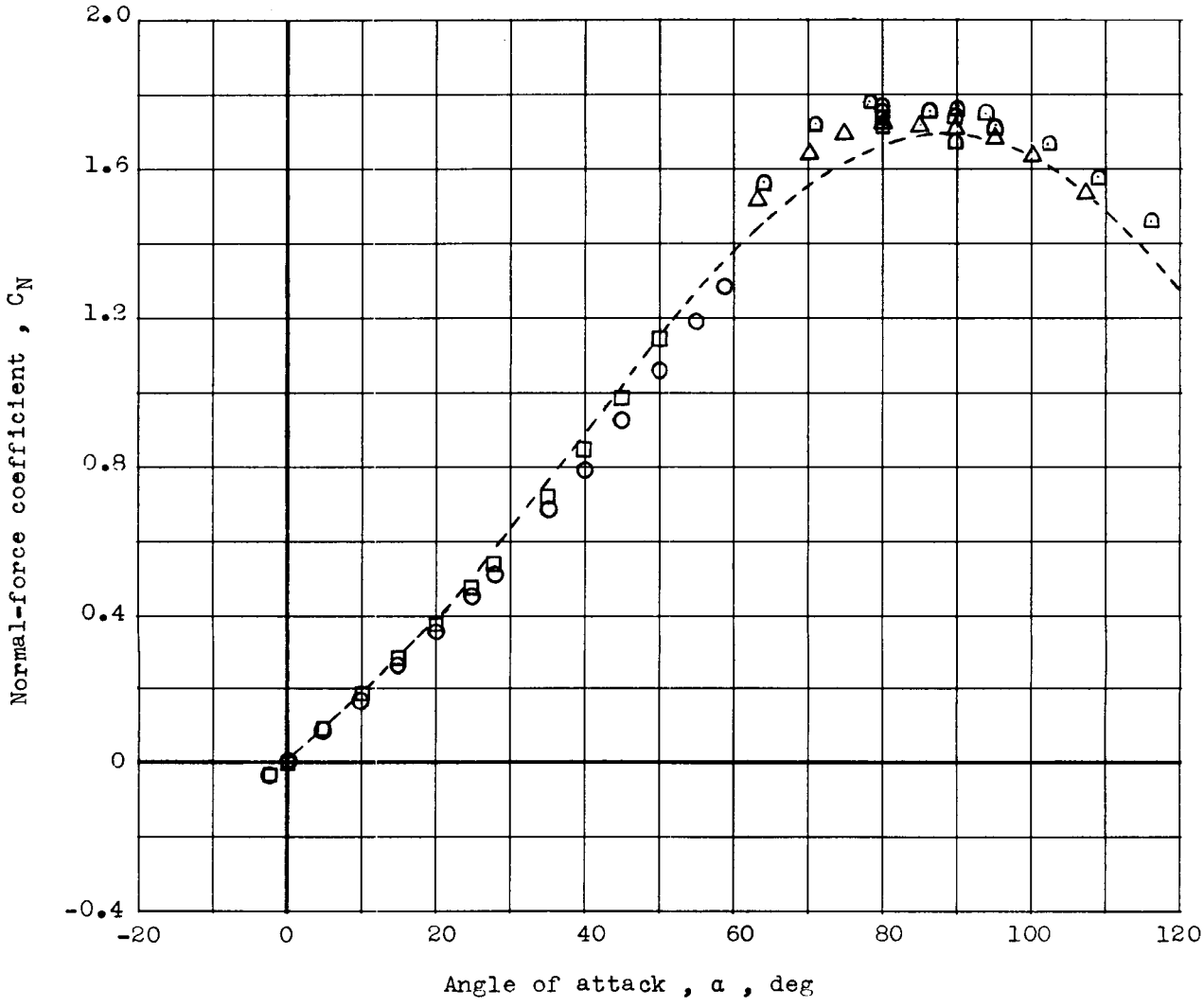

Figure 4.- Variation of normal-force coefficient with angle of attack with a modified Newtonian theory shown for comparison.

		M	R
Model 1,	○	6.6	0.18×10^6
	□	6.7	0.45×10^6
Model 2,	⌂	6.7	0.15×10^6
	△	6.7	0.19×10^6
Theory	-------	7.0	Modified Newtonian

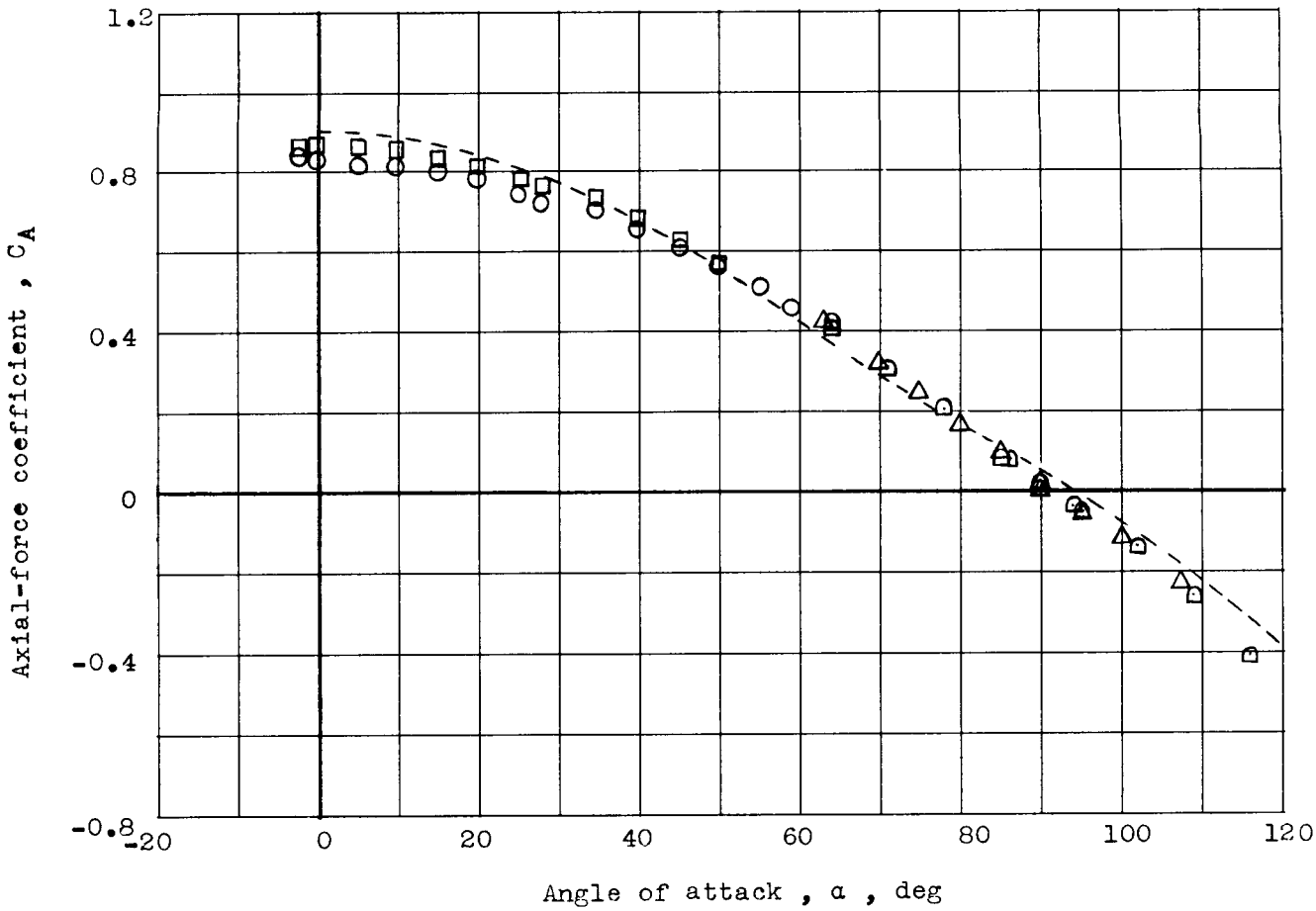

Figure 5.- Variation of axial-force coefficient with angle of attack with modified Newtonian theory shown for comparison.

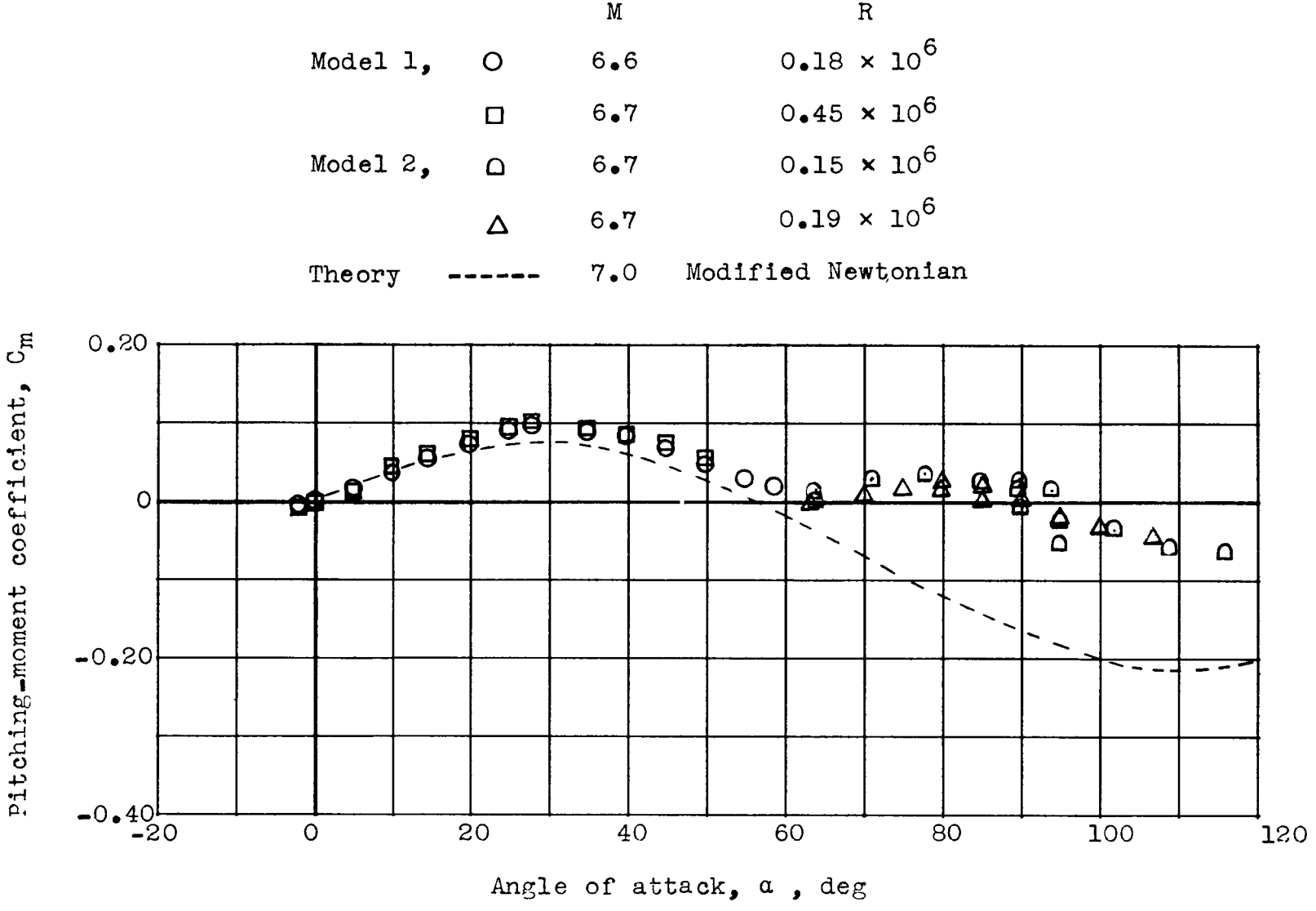

Figure 6.- Variation of pitching-moment coefficient with angle of attack as compared with a modified Newtonian theory.

		M	R
Model 1 ,	○	6.6	0.18×10^6
	□	6.7	0.45×10^6
Model 2 ,	⌂	6.7	0.15×10^6
	△	6.7	0.19×10^6
Theory	-------	7.0	Modified Newtonian

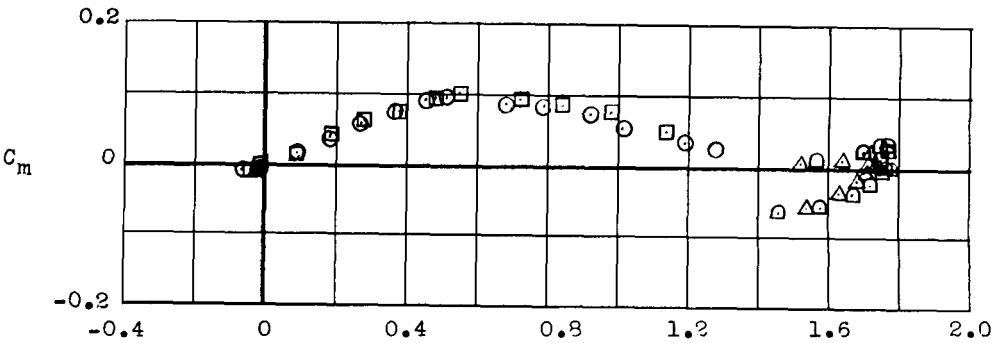

(a) Variation of pitching-moment coefficient with normal-force coefficient for the empty center-of-gravity location.

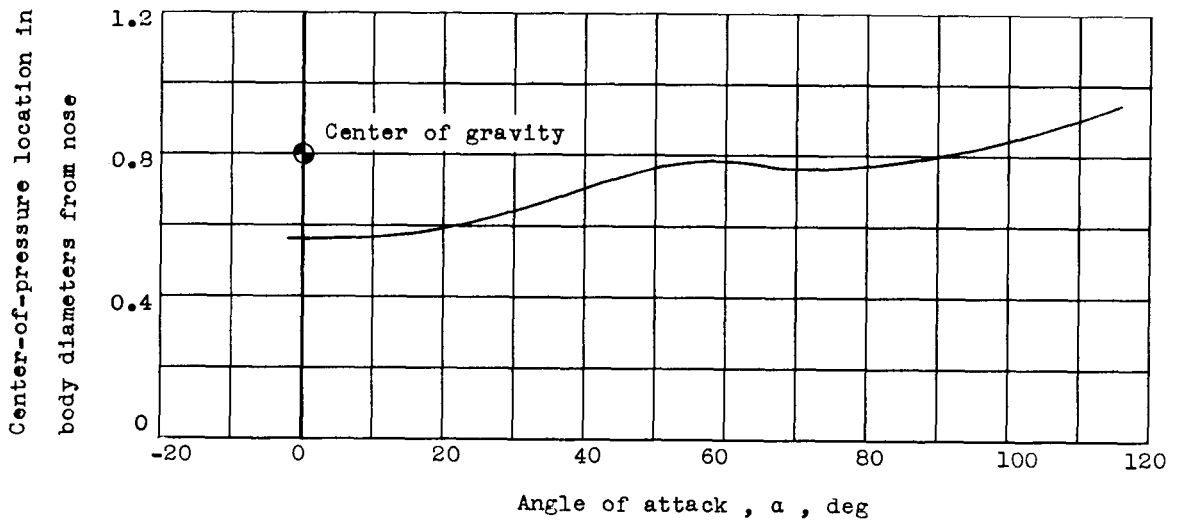

(b) Location of pressure centroid for various angles of attack.

Figure 7.- Variation of pitching-moment coefficient with normal-force coefficient and center of pressure with angle of attack.

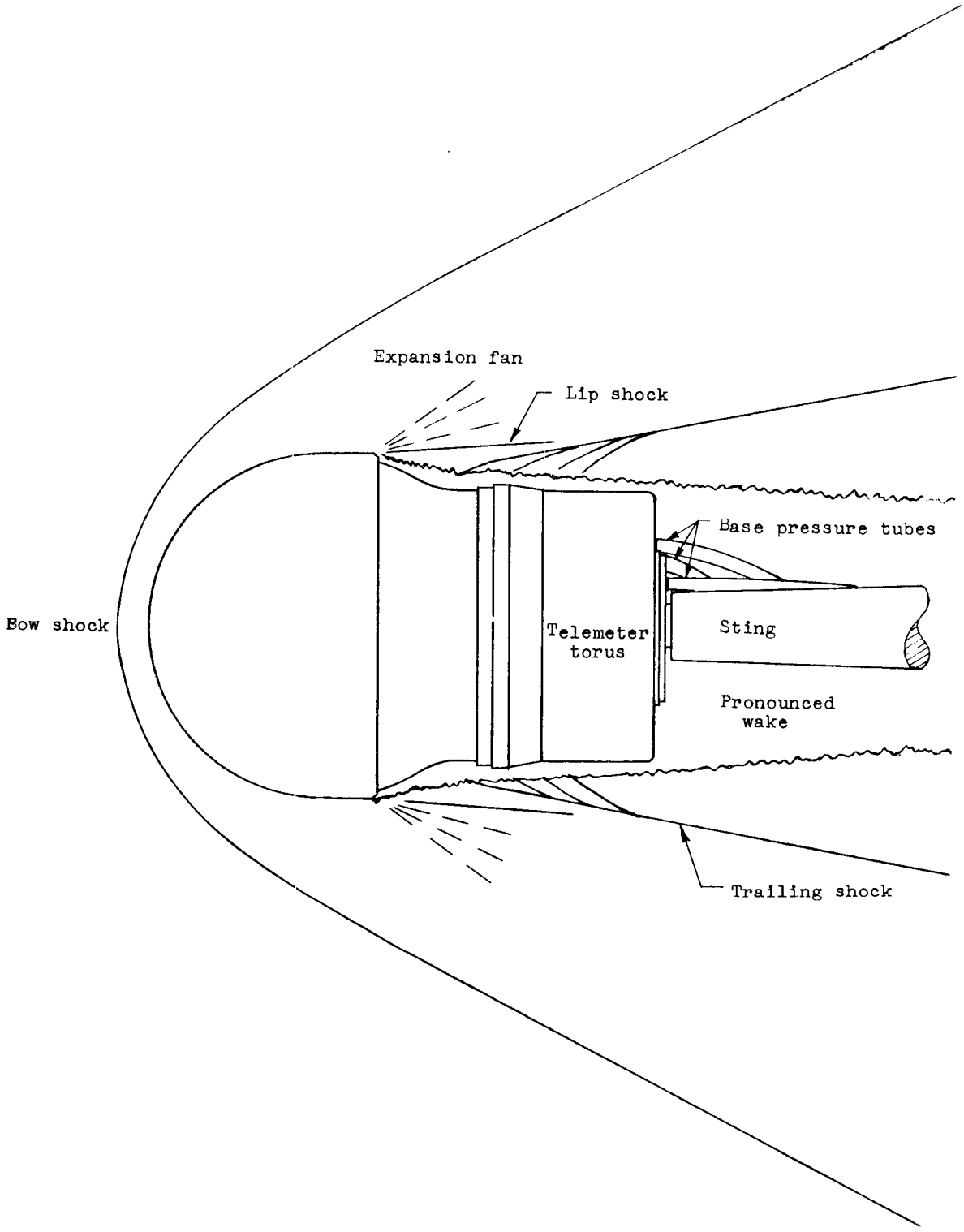

Figure 8.- Sketch of schlieren photographs of model 1 at $M = 6.7$ and $R = 0.45 \times 10^6$ in air. Various elements of the flow in the region of the telemeter torus are identified.

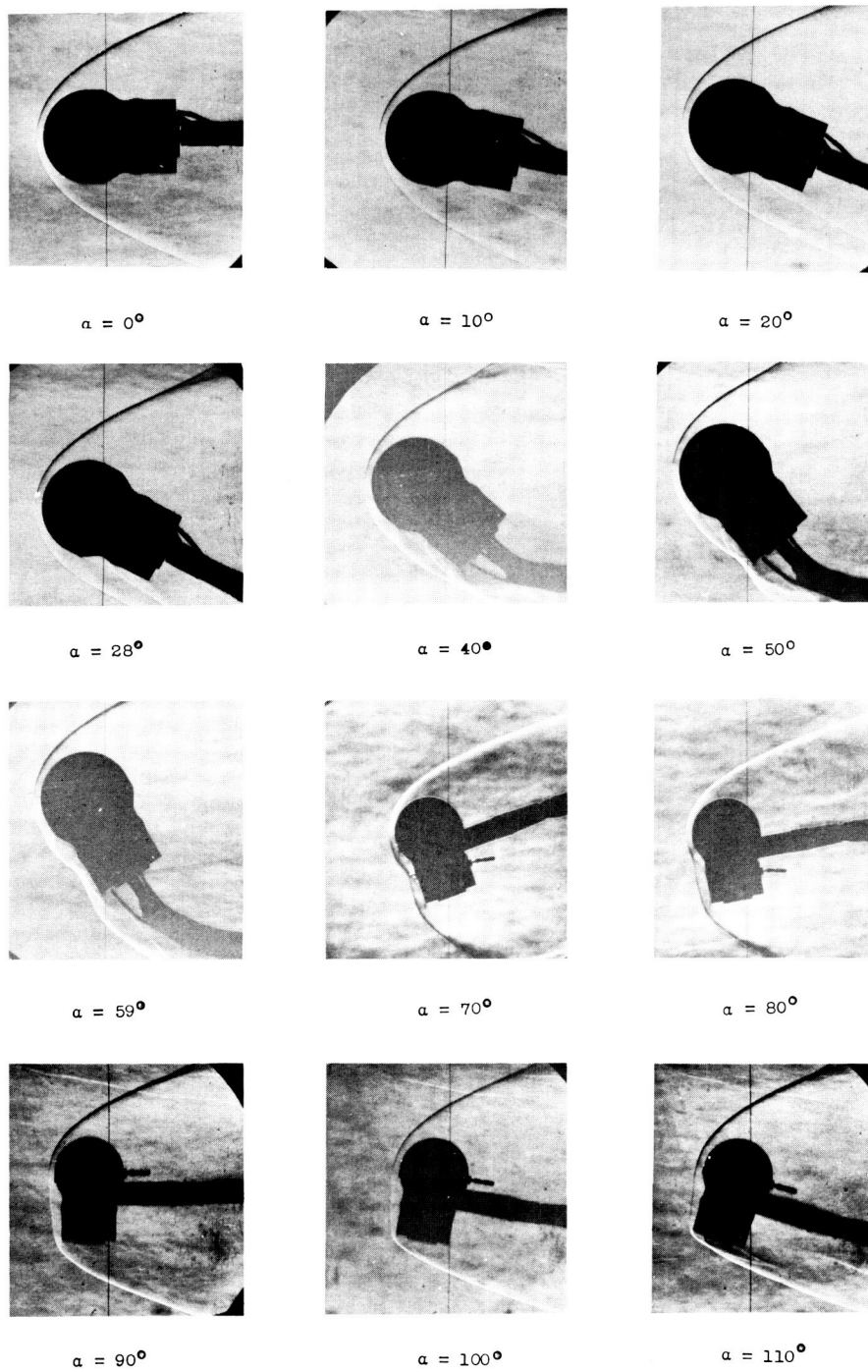

L-63-3115

Figure 9.- Schlieren photographs of models 1 and 2 near M = 6.7 in air illustrating the variation of shock-wave formation with angle of attack.

Legend

Position	Event
1	First-stage burnout
2	Second-stage burnout
3	Third-stage burnout
4	Trajectory of spin-stabilized velocity package
5	Fourth-stage ignition
6	Fourth-stage burnout
7	Fifth-stage ignition
8	Fifth-stage burnout
9	Sixth-stage ignition
10	Sixth-stage burnout
11	Reentry body trajectory

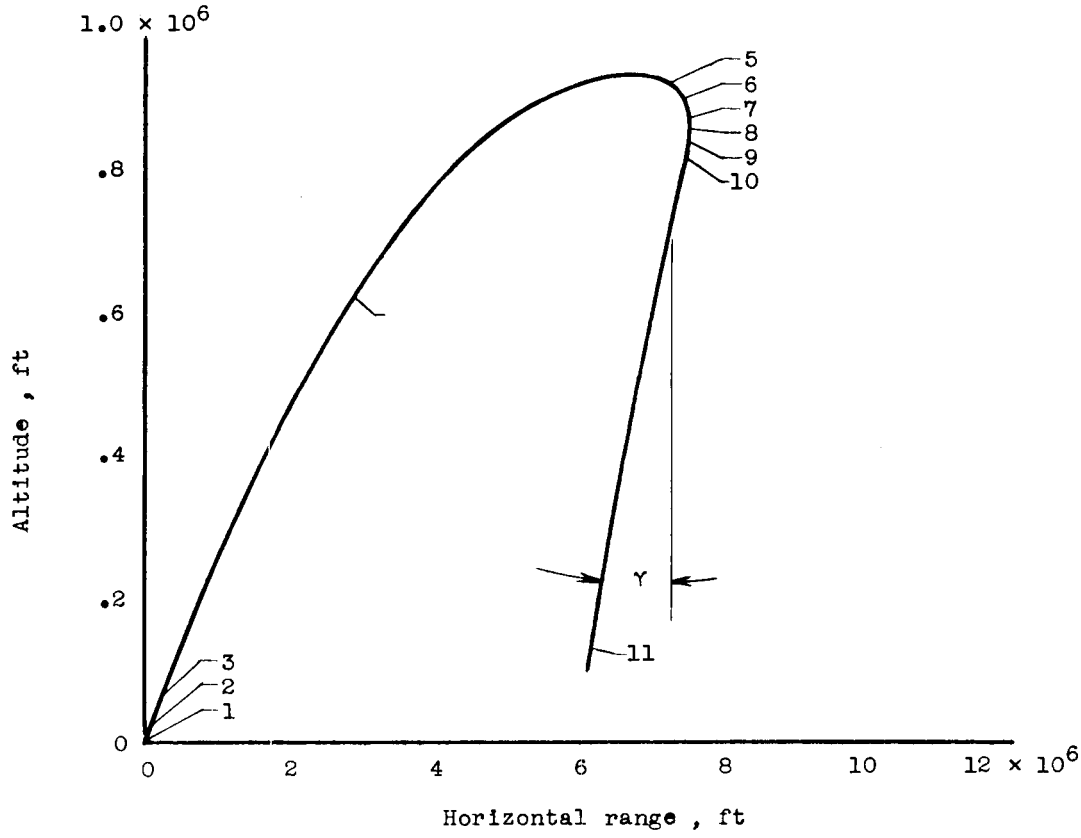

Figure 10.- An illustration of the unusual Trailblazer I trajectory.

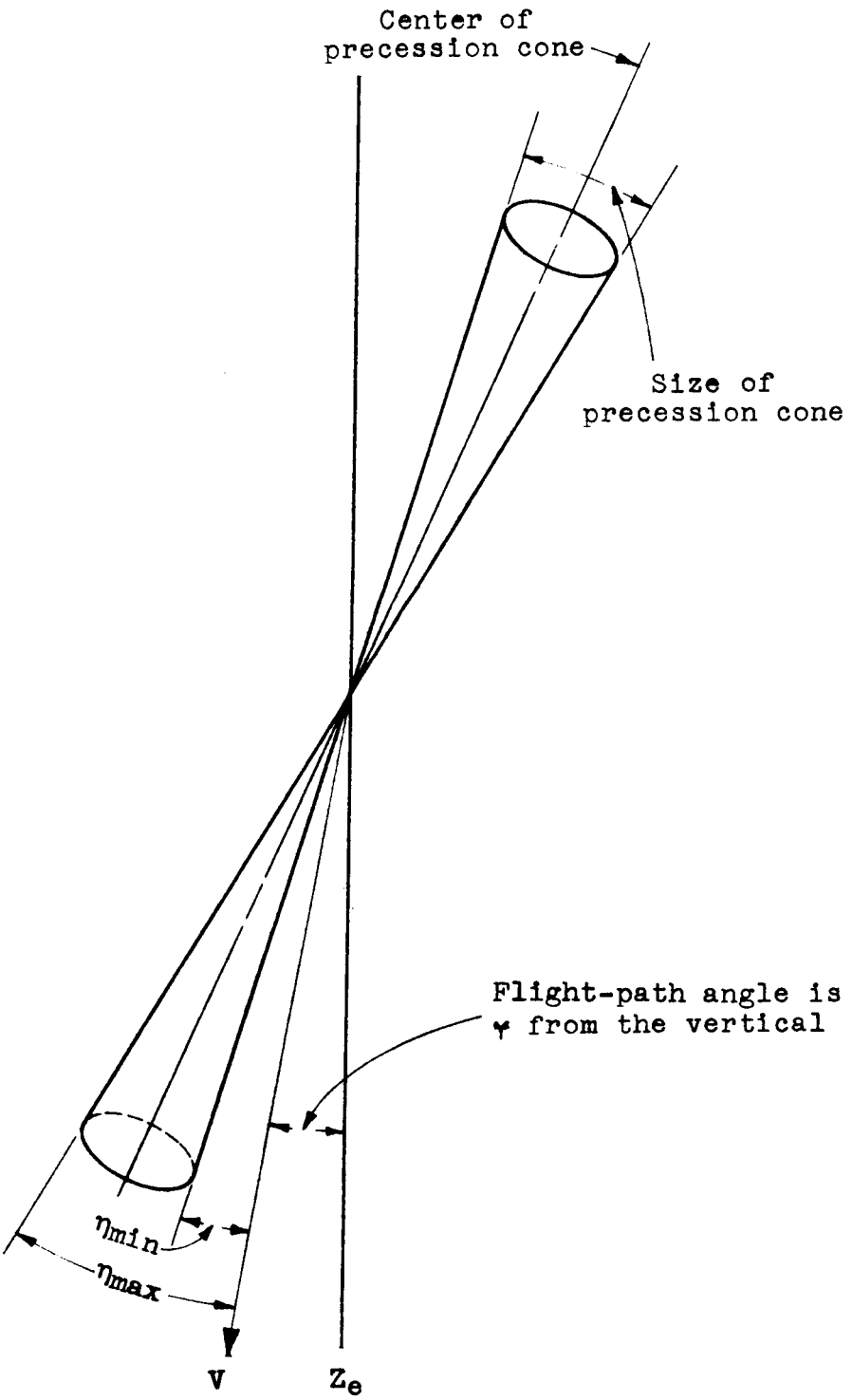

Figure 11.- Sketch of initial conditions to show some of the initial precession conditions without nutation.

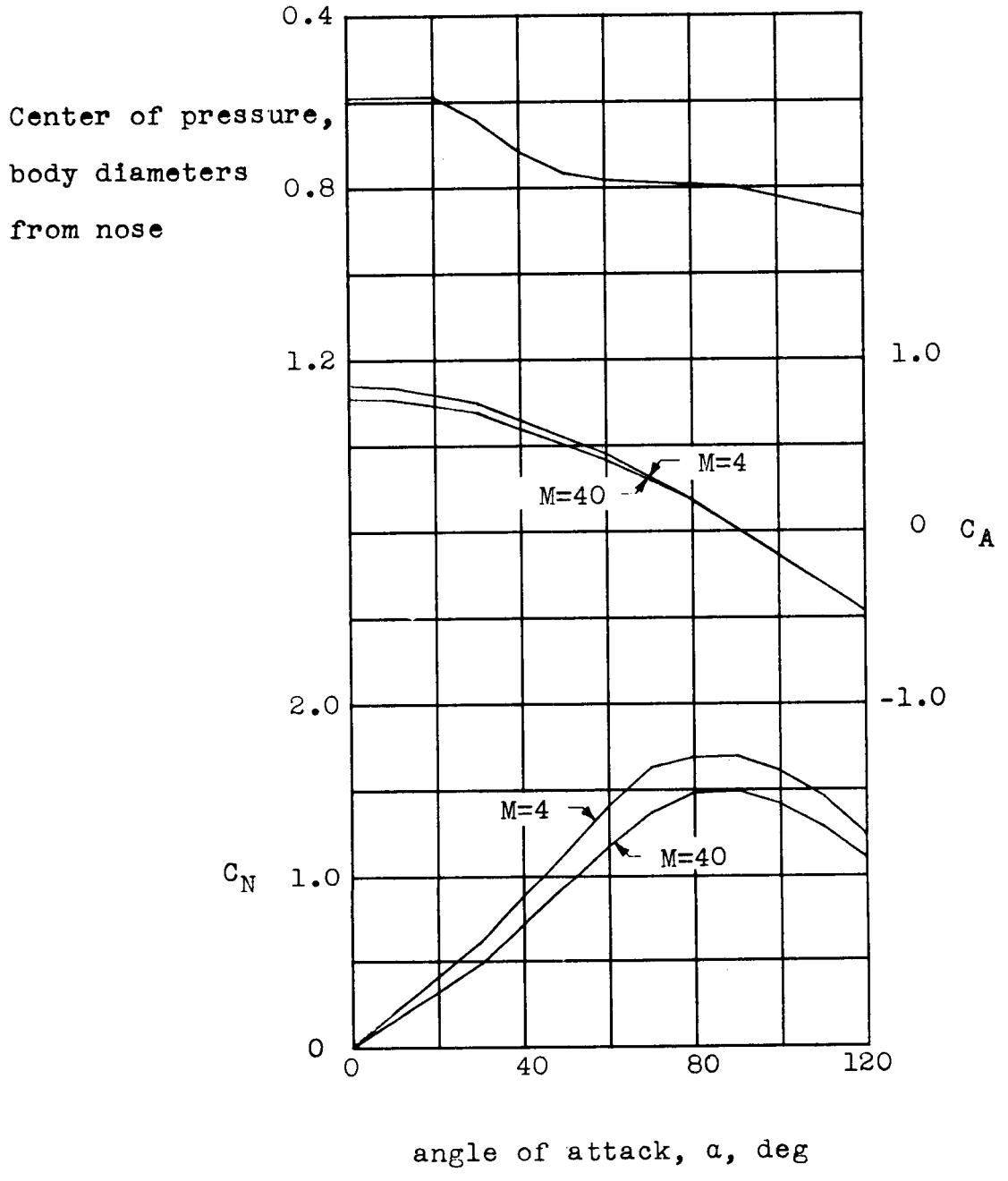

Figure 12.- Illustration of the straight-line assumptions used to put center of pressure, C_A, and C_N into computer program as a function of both Mach number and angle of attack.

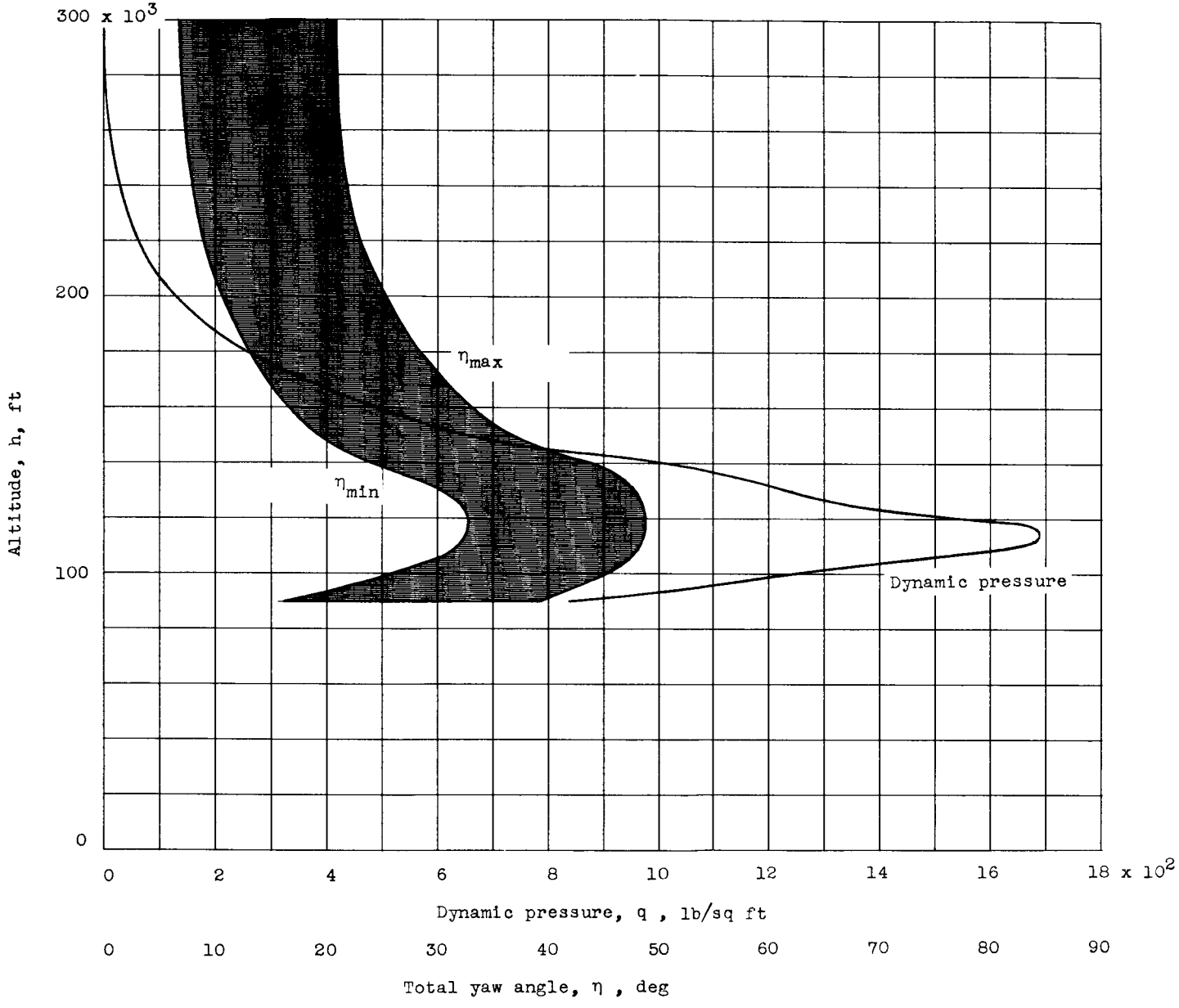

Figure 13.- Variation of the maximum and minimum total yaw angle and dynamic pressure with altitude to illustrate the gradual buildup of the aerodynamic effects.